Second-chance speciation in the Clouded Apollo butterfly

J. Lancho-Silva, L. Spilani, V. Marques, C. Bruschini, V. Dincă, M. Mutanen, M. Franzén, D.C. Adams, L. Dapporto, R. Vila

In brief

Lancho-Silva et al. reveal two successive contacts between butterfly populations that capture the surprisingly rapid emergence of reproductive isolation driven by selection for chemical differences, a mechanism rarely documented in action. Their work demonstrates that Europe's protected Clouded Apollo butterfly actually comprises two distinct species, with implications for conservation.

Highlights

- Genomics reveal that Europe's iconic Clouded Apollo butterfly includes two species.
- An ancient contact with gene flow formed the admixed Pyrenean populations.
- In the current contact, full reproductive isolation is linked to chemical differences.
- A case of recent chemical speciation with profound consequences for conservation.

1. INTRO/SUMMARY FOR CURRENT BIOLOGY:

Contact zones, where genetic lineages meet, provide a unique opportunity to study speciation and reveal how reproductive barriers emerge (1-3). However, species ranges are dynamic, contact zones may be ephemeral (4-5), and reinforcement—selection against hybrids—is a particularly elusive phenomenon (6-8). We use an integrative approach—genomic, chemical, and morphological data coupled with ecological and demographic modeling—to evaluate lineage limits, reconstruct contact history, and infer reproductive isolation strength and mechanisms in the protected Clouded Apollo butterfly (*Parnassius mnemosyne*) in Europe (9). The status of this taxon is highly debated: a potential cryptic species (*Parnassius turatii*) edging *P. mnemosyne* sensu stricto in the Eastern Alps has been proposed, yet evidence remains inconsistent in the absence of genomic data (10-18). We reveal the presence of two genetic lineages that diverged about 0.8 million years ago and experienced two successive episodes of secondary contact. During the last glaciation, the lineages met in western Europe, resulting in admixture and the formation of hybrid Pyrenean populations before reproductive isolation had evolved. In contrast, genomic data show no detectable gene flow at their present-day contact in the Eastern Alps, despite morphological and ecological similarity. Evidence of mutual chemical character displacement at this contact provides compelling evidence for bidirectional

reinforcement in action. Collectively, these findings portray a system in which lineages that once exchanged genes now re-encounter each other and reproductive isolation is generated—a second chance for speciation to succeed—and demonstrate that the Clouded Apollo comprises two cryptic species, with direct implications for EU legislation implementation and IUCN assessments (9, 19,20,21).

2. RESULTS:

Genome-wide markers resolve two species with a sharp boundary at the contact zone

Analyses based on genomic data consistently separated *P. mnemosyne* and *P. turatii* into two well-supported genomic clusters. The phylogenetic analysis recovered two major clades corresponding to *P. mnemosyne* and *P. turatii*, with high support; one group was represented by samples from Spain, France, the Apennines (including Sicily), and the Eestern/central Alps, while the remaining *P. mnemosyne* formed a distinct clade (Fig.1 A.1). Principal component analysis (PCA) segregated individuals by species and geography, with PC1 (>18% variance) separating samples on either side of the contact zone and placing a small number of peripheral individuals intermediate, indicating potential ancestral admixture outside the current contact (Fig.1 C1-2). Bayesian ancestral clustering analysis cleanly separated the species with no admixture at the current contact despite ~40 km proximity, while the best supported was K = 3, which further subdivided *P. mnemosyne*; K = 4 identified the Pyrenean population as a discrete lineage (Fig. A.2; Supplementary). Geographic overlays of ancestry proportions reinforced strong phylogeographic structure across Europe (Fig. 1, B.1-2). Overall, the main contact zone shows strict genomic integrity between species, with only minor peripheral introgression.

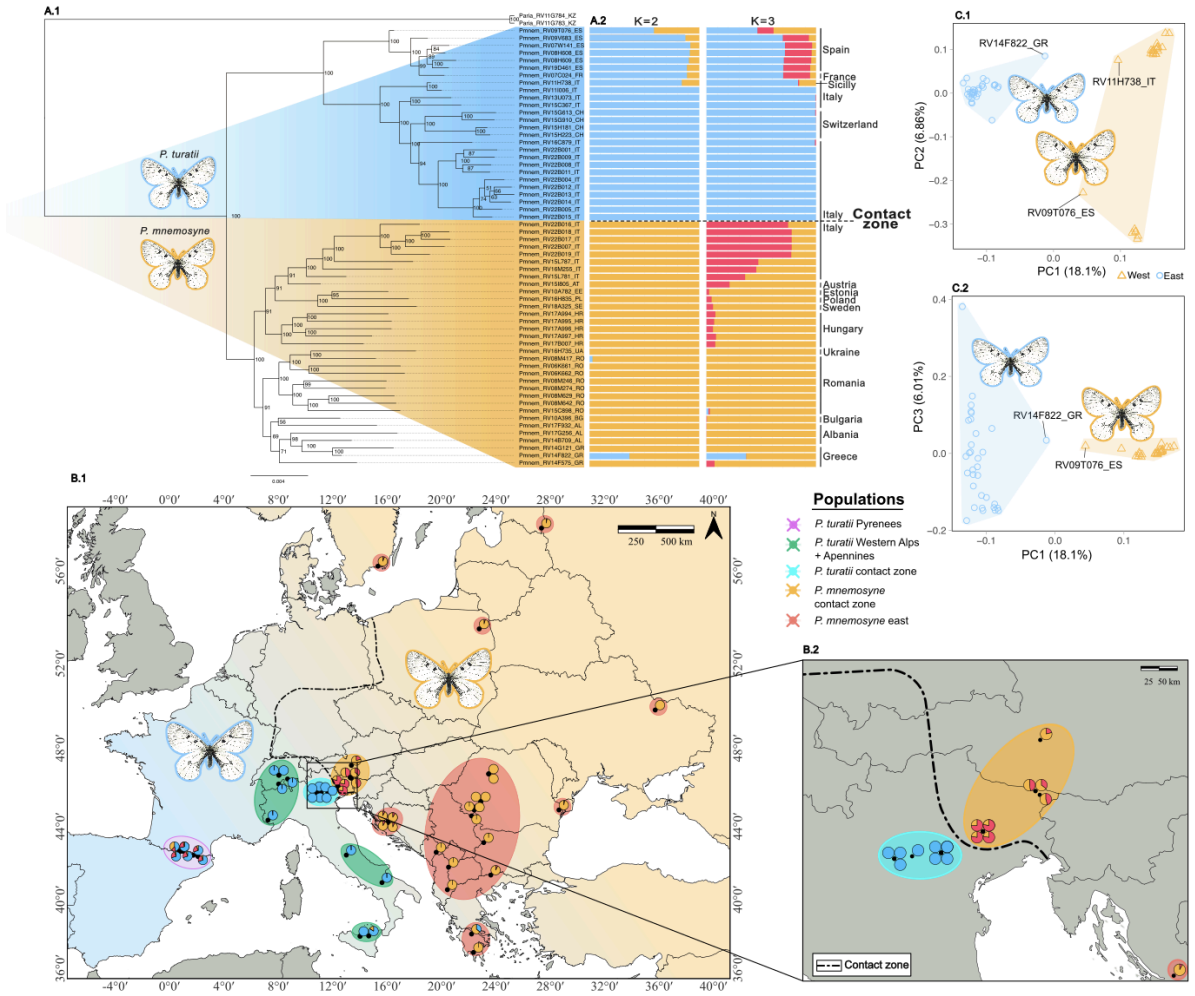

Figure 1. Phylogenetic, population structure, and geographic analyses of the Clouded Apollo butterfly in Europe. (A.1) Maximum likelihood phylogenetic tree showing two well-supported clades corresponding to the cryptic species *P. turatii* and *P. mnemosyne*. (A.2) STRUCTURE results at K = 2 and K = 3, represented as bar plots showing individual ancestry proportions. (C.1&2) Principal component analyses (PCA) based on SNP data: PC1 vs. PC2 (top) and PC1 vs. PC3 (bottom); individuals with potentially admixed genomes, consistent with STRUCTURE results, are indicated. (B.1&2) STRUCTURE results at K = 3 represented as pie charts overlaid on a geographic map, showing ancestry proportions per sampling locality; the zoom corresponds to the current contact zone in the Eastern Alps. Dashed line indicates the western limit of the distribution of P. mnemosyne sensu stricto, according to Bolotov et al., 2021.

Contemporary gene flow is absent at the Alpine contact zone, but historical introgression into Pyrenean *P. turatii* is supported

Gene flow tests (D-statistics) across different population configurations revealed no detectable gene flow between contact-zone *P. mnemosyne* and *P. turatii*. In contrast, significant gene flow between *P. mnemosyne* from the contact zone and Pyrenean *P. turatii* was detected (p = 0.0036; Fig. 2, A.1-2), despite the large geographic distance between these populations. Although surprising given current distribution ranges, this result is consistent with STRUCTURE clustering signals of admixture in the Pyrenees. One individual from Sicily and one from the Peloponnese also showed signals of potential ancestral admixture, but this hypothesis could not be confirmed due to limited sample sizes. Across all individuals screened, no *Wolbachia* infection was detected, arguing against cytoplasmic incompatibility as a player in reproductive isolation.

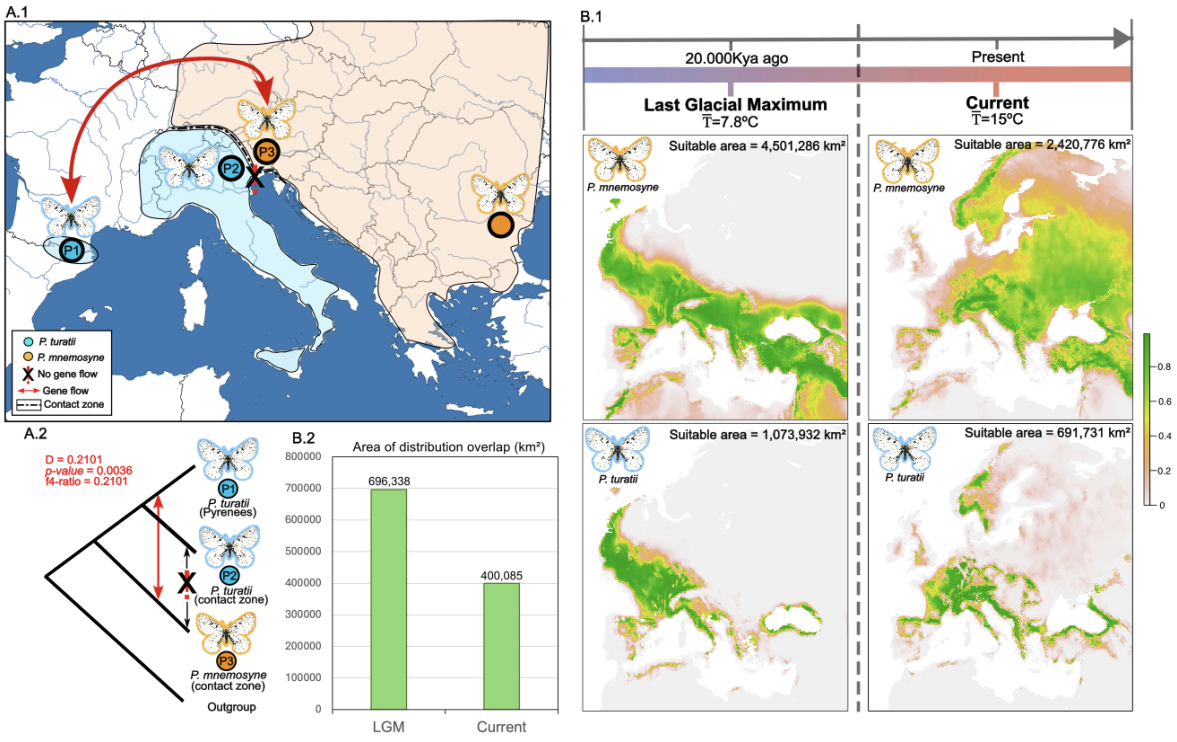

Figure 2. Ecological niche modelling and demographic history of *P. mnemosyne* and *P. turatii*. (A.1) Map showing the geographic distributions of the populations used in the D-statistics gene flow tests, with arrows indicating detected gene-flow events and crossed exclamation marks indicating no evidence of gene flow. (A.2) Schematic tree summarizing the relationships among the analysed populations and the inferred interspecific gene-flow events. (B.1) Ecological niche model projections for *P. mnemosyne* and *P. turatii* during the Last Glacial Maximum (LGM) and under current climatic conditions. (B.2) Estimated area of potential distribution overlap between the two species (in km²) under LGM and present-day climatic scenarios.

Glacial-cycle dynamics created opportunities for secondary contact; demographic models quantify divergence and asymmetric gene flow

Ecological niche models (ENMs) indicate some overlap of suitable areas for the two species. However, potential suitable areas are markedly different in their continuity: *P. mnemosyne* shows a more continuous, northeasterly-extended suitability (current suitable area ≈ 2,420,776 km²), whereas *P. turatii* is fragmented and mostly confined to a few Mediterranean and adjacent montane regions (≈ 691,731 km²; Fig. 2, B.1, "Current"). During the Last Glacial Maximum (Fig. 2, B.1, "LGM"; ~20 ka, mean T ≈ 7.8 °C), both species were unable to occupy the completely glaciated northern Europe. We infer that, during this period, *P. mnemosyne* occupied large refugial belts in the Balkans/Black Sea–southern Carpathians–Caucasus foothills and dispersed into western Europe (≈ 4,501,268 km²). *P. turatii* potentially persisted in Iberia and the central Mediterranean, but the main suitable refugium was located in western Europe, from the Atlantic coast of France to the Alps (≈ 1,073,932 km²; Fig. 2, B.1, "LGM"). The potential distributional overlap of the two species almost doubled at the LGM—from ~400,085 km² today to ~696,338 km² (≈ 1.74× increase; Fig. 2, B.2)—representing an absolute gain of ~296,253 km² where interspecific encounters were potentially more likely. The main area of overlap was recovered in western Europe, which is the main potential refugium for both lineages and the area where the first contact likely occurred during the last glaciation.

Demographic inference revealed a first split at ~820 kya, with a subsequent secondary split within *P. turatii* at ~154 kya, and unidirectional gene flow from *P. mnemosyne* into Pyrenean *P. turatii* (Fig. 3); alternative models invoking bidirectional exchange, hybrid origin, no gene flow, or alternative topologies fit substantially worse (Supplementary). The quantitative spatial–temporal concordance between ENM-inferred LGM overlap and demographic modeling estimates supported historical secondary contact with asymmetric introgression in the Pyrenees (Fig. 2-3).

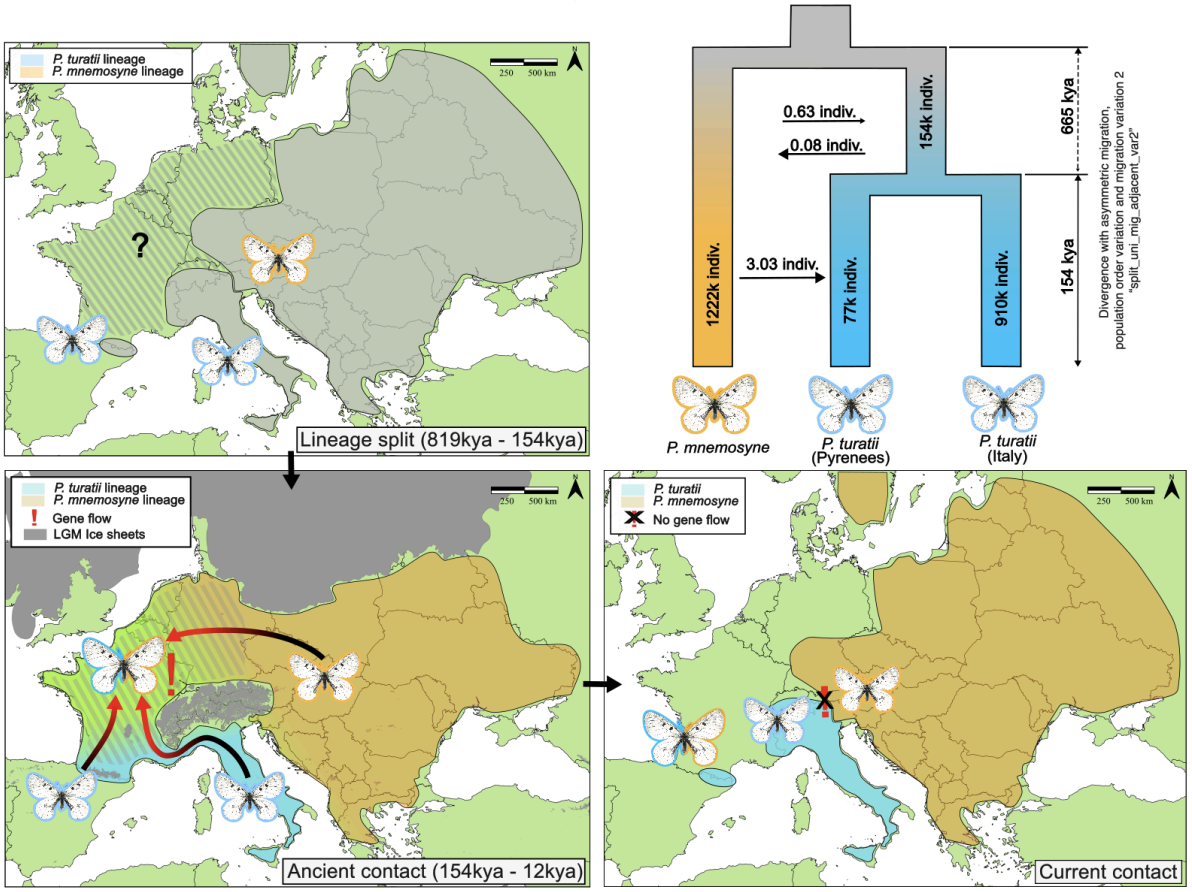

Figure 3. Demographic model and inferred evolutionary history of *P. mnemosyne* and *P. turatii*. The best-fit demographic model (top right) supports an initial evolutionary split (~819 kya) followed by a later divergence within *P. turatii* (~154 kya). Lineage relationships are shown, with arrows indicating the direction and relative magnitude of inferred gene flow. Maps illustrate the three inferred phases: (1) lineage split, showing potential but unknown early allopatric ranges; (2) ancient contact (154 kya–12 kya), when glacial-period expansions increased geographic overlap and enabled secondary contact; and (3) present-day contact, where a sharp boundary and no current gene flow are detected.

Wing-scale morphology separates species and shows displacement in Pyrenean *P. turatii*

Geometric morphometrics of forewing scales (Fig. 4A)—a character previously suggested to have diagnostic value in this system (Bolotov et al., 2021)— revealed differences in shape correlating with species across their range: PCA captured 71.56% (PC1) and 16.66% (PC2) of variance, with allopatric *P. mnemosyne* skewed to negative PC1 and *P. turatii* (western Alps, Apennines and Pyrenees) to positive PC1. Nevertheless, contact-zone individuals were intermediate regardless of their genetic lineage (Fig. 4C). Statistical tests detected a significant group effect ($F = 12.07$, $Z = 6.4323$ $p = 0.001$;

~19% variance explained, Supplementary). Pairwise tests among groups showed that allopatric *P. mnemosyne* differed from all *P. turatii* groups ($p \leq 0.003$), with Pyrenean *P. turatii* the most divergent ($p \leq 0.003$ vs. all others); differentiation between *P. mnemosyne* and *P. turatii* at the contact zone was marginal ($p = 0.054$) (Supplementary). Deformation grids indicated narrower, elongated scales in *P. mnemosyne* and broader, more curved scales in *P. turatii* (Fig. 4B), with the Pyrenean lineage showing the greatest lateral divergence (Supplementary).

Cuticular hydrocarbons (CHCs) show peak discrimination in sympatry and decline with distance, consistent with reinforcement

In total, 43 cuticular hydrocarbon (CHCs) compounds were identified from the wings of *P. turatii* and *P. mnemosyne* males, comprising a mixture of straight-chain alkanes, methyl-branched alkanes, and monoalkenes (Supplementary Table S10). Our chemical analyses (Fig. 4A) revealed separation between species overall, although individuals collected in the contact zone showed much clearer chemical differences: *P. turatii* and *P. mnemosyne* from from the contact zone in the Eastern Alps occupied distinct regions of the first two PCA axes of chemical composition indicating the highest divergence between populations (Fig. 4D). The compounds mostly associated with *P. turatii* are the three methyl-branched alkanes (3-MeC25, 13-MeC33, and 3Me-C36), while those associated with *P. mnemosyne* include specific isomers of three monoalkenes: C25:1 (isomers a and b), C29:1 (isomers a and b), and C33:1 (isomer b). Classification accuracy in a Partial Least Square Discriminant Analysis for these contact populations was correspondingly high—96.0% for contact zone *P. turatii* and 100% for contact zone *P. mnemosyne*. In contrast, accuracy was much lower for populations farther from the contact zone (66.7% in non-contact *P. mnemosyne*, 63.6% in Pyrenean *P. turatii*, and 64.3% in western Alps–Italian Peninsula *P. turatii*; Supplementary Table S8).

Pairwise interspecific CHC distances declined significantly with increasing distance from the contact zone in both species (Fig. 4E, Supplementary Table S10), consistent with symmetric character displacement. Species-specific models showed a similar decline in *P. turatii* (slope = -0.00314 ± 0.00116 SE, $p = 0.0069$) and in *P. mnemosyne* (slope = -0.00244 ± 0.000 SE, $p = 0.0048$), thus producing a "mirror-like" pattern of strong chemical differentiation at the contact that weakens with distance.

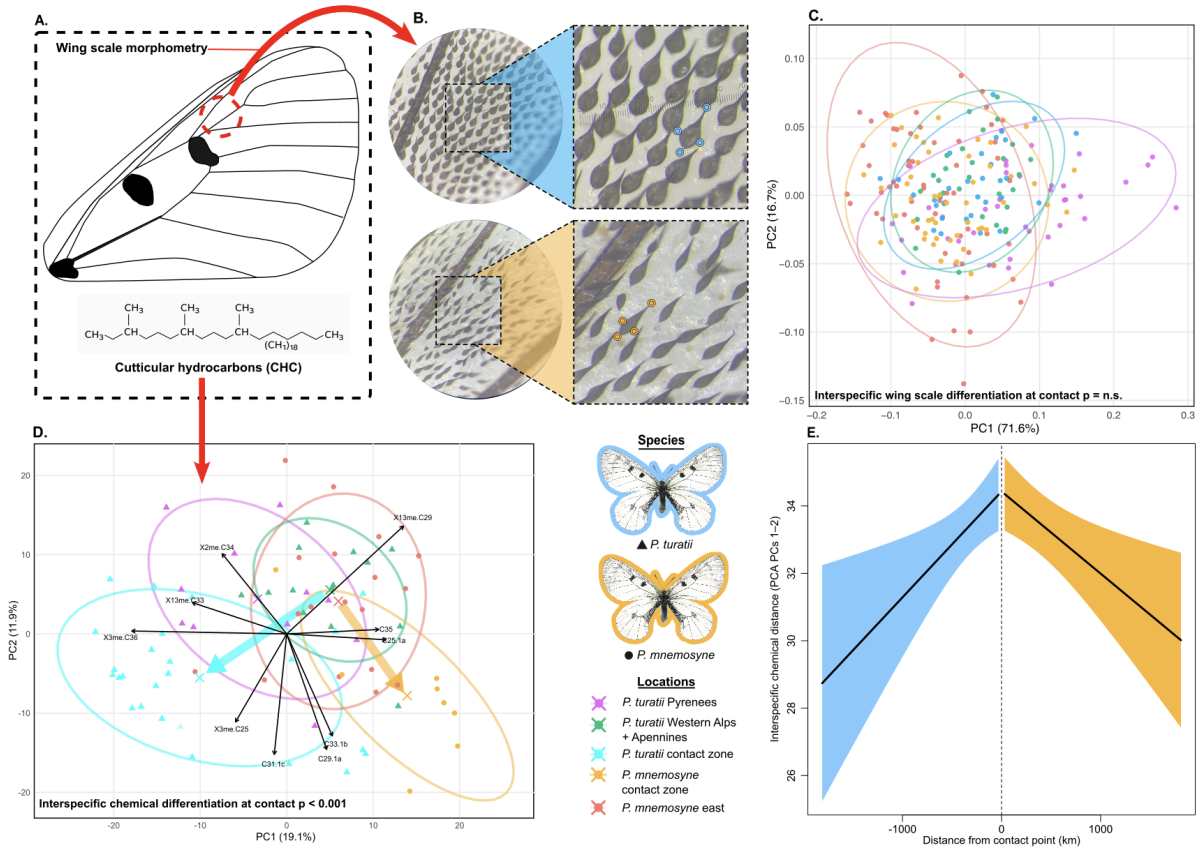

Figure 4. Morphological and chemical divergence between *P. mnemosyne* and *P. turatii*. (A) Schematic forewing showing the location of sampled scales and an example CHC compound. (B) Representative scale morphology of *P. mnemosyne* (blue) and *P. turatii* (orange). (C) PCA of scale shape (PC1 = 71.56%, PC2 = 16.66%). (D) PCA of CHC profiles reveals partial overall separation but pronounced discrimination in contact-zone populations, with key compounds (vectors) driving species chemical divergence. Colored arrows show chemical shifts by linking the centroids of non-contact populations to their conspecific contact-zone population. (E) Plot of interspecific CHC distance versus geographical distance to the current contact zone in the Eastern Alps.

3. DISCUSSION:

The lack of gene flow at the contact zone in the Eastern Alps demonstrates that *P. mnemosyne* and *P. turatii* have completed speciation despite their recent divergence and long-standing ecological similarity.

The concordance between gene flow patterns, ancestral clustering analyses, demographic inference, and paleoclimate-based range reconstructions supports a coherent evolutionary scenario for this system. An initial lineage split about 0.8 Mya separated the ancestors of *P. turatii* and *P. mnemosyne*, after which they likely diverged in allopatry for most of the time, although with some degree of gene

flow. During the last glacial period (154–12 kya), both cold-adapted lineages expanded, most notably the ancestor of *P. mnemosyne* across western Europe, reaching the Atlantic. These expansions brought the species into contact in western Europe, where they interbred and contributed to the admixed ancestry of today's Pyrenean populations. With the onset of interglacial warming, both lineages retracted to their respective refugia, reducing contact and allowing isolated populations to advance in the speciation process. Finally, upon their most recent secondary contact—represented by the current contact zone in the Eastern Alps—the lineages now no longer hybridize.

This system illustrates the view of speciation as a continuum, the final step of which usually takes place under secondary contact (Mallet et al., 2007; Shawk & Mullet, 2007; Lowry & Gould, 2016; Stankowski et al., 2021), and provides a rare empirical example of what can be considered "second-chance speciation": A first failed opportunity for speciation during the last glaciation, in which gene flow dominated and the lineages fused, and a second successful one, in the current contact zone, where the clash between the forces of selection and admixture resulted in speciation. Genomic analyses provide us with the capacity not only to test for speciation in contemporary contact zones, but also to infer ancestral events of sympatry and their outcome. It is likely that, given the repetitive Quaternary climatic oscillations, lineages had multiple contacts across recent evolutionary history, and each of them provided a chance for gene flow and reinforcement to act, and for speciation to complete. In the case of the Clouded Apollo cryptic species, we cannot rule out the existence of additional contact events in the past. In fact, the demographic model suggests bidirectional gene flow across their history, and a few specimens in Sicily and the Peloponnesus suggest potential ancestral admixture. How frequently contact events result in speciation is unknown, but we hypothesize that these cases represent a conspicuous minority, while lineage fusion may be a much more common outcome whose signal dilutes with time.

Although the multiple Quaternary climatic oscillations produced highly dynamic distribution shifts in many mobile organisms, the signal of which becomes erased by newer events, this temporal contrast directly illustrates how changing climatic regimes can repeatedly open and close opportunities for hybridization, thereby shaping evolutionary trajectories (Taberlet et al., 1998; Hewitt, 2004; Schmitt et al., 2007; Marques et al., 2024; Dapporto et al., 2024). The lack of *Wolbachia* infections argues against cytoplasmic incompatibility caused by these endosymbiotic bacteria, while prior reports of minor genital differences (Bolotov et al., 2021) underscore that premating mechanical isolation remains untested but is unlikely to be the main factor. Earlier inferences of introgression based on a small number of highly polymorphic microsatellites (e.g., steep clines in the mid-Piave Valley, North-Eastern Italy: Gratton et al., 2025) can be reconciled with our genome-wide results by differences in marker resolution and sampling scale.

A key mechanism that plausibly finalized reproductive isolation is reinforcement. Cuticular hydrocarbon (CHC) profiles show pronounced, localized displacement at the contact zone without accompanying genomic admixture—an expected signature when selection against maladaptive

hybridization strengthens premating cues. The apparent mutual displacement across species, together with the decay of CHC divergence away from the contact, argues that chemical signaling now functions as a mating barrier refined during or after past contact. This interpretation aligns with broader evidence that speciation in Lepidoptera can be completed through premating barriers even in the absence of large ecological niche shifts **(**Kozak et al., 2015; Schmitt & Hewitt, 2004**)**. Chemical communication is widespread in butterflies and is a well-established component of mate recognition. However, to our knowledge, this is the first documented case in European butterflies where both species show chemical divergence that reaches its maximum in sympatry. Behavioral choice tests with synthetic blends, female-focused CHC sampling, and transcriptomic analyses of pheromone biosynthesis genes are logical next steps to establish causality and directionality (Li et al., 2017; Ehlers and Schulz, 2023; Ômura et al., 2020; Chen et al., 2021; Liénard et al., 2014).

Despite the present-day overlap in environmental niches, the two species retain distinct evolutionary identities. Their similar environmental requirements indicate that ecological divergence was not the primary driver of speciation. Instead, we propose that historical allopatry, episodic secondary contact, and reinforcement jointly shaped the divergence of *P. turatii* and *P. mnemosyne* (Kozak et al., 2015; Schmitt & Hewitt, 2004). The morphological divergence detected in wing-scale shape, including clinal convergence near the contact zone, indicates phenotypic evolution along axes only weakly coupled to genome-wide ancestry and plausibly influenced by local environmental conditions such as montane humidity and UV exposure. Although previous taxonomic proposals are consistent with these differences (Bolotov et al., 2021), they are not reliable diagnostic traits, as these differences disappear in the contact zone, where the two species can most likely be misidentified.

Because the Pyrenean populations are currently allopatric, their level of reproductive isolation cannot be determined. Although multiple hypotheses remain possible, we treat these populations as *P. turatii*, since only a small portion of their genome shows introgression from *P. mnemosyne,* and the phylogenetic analysis groups them with *P. turatii*. However, they are genetically distinct from populations in the Alps, Apennines, and Sicily and should be recognized at least as a subspecies. As the Pyrenees are the type locality *turatii* Fruhstorfer, 1908 —name that has priority (Cotton et al., 2021)—, we propose two subspecies within *P. turatii*: *P. turatii turatii* Fruhstorfer, 1908 **comb. nov.** for the Pyrenean populations, and *P. turatii parmenides* Fruhstorfer, 1908 **comb. nov.** (type locality: Maritime Alps) for the remaining populations.

Recognizing *P. mnemosyne* and *P. turatii* as distinct species, and dividing the latter into two subspecies, has important conservation consequences. The redefinition of species boundaries reduces the effective distribution of each taxon, particularly *P. turatii*, which has highly localised and low-density populations that occupy fragmented montane habitats highly vulnerable to climate warming (Araujo & Luoto 2007). For example, in the Catalan Pyrenees, where it is locally protected and constantly monitored, population density has dramatically declined (-95.3% from 2006 to 2025) and is apparently extinct in some regions (CBMS: https://www.catalanbms.org/en/especies/pappmn,

2025). Similarly, several Apennine populations seem to be on the brink of extinction (Cini et al., 2020). Nevertheless, *P. mnemosyne* is also facing remarkable declines and extinctions in northern Europe (Bolotov et al., 2013; Westin et al., 2018; Franzén & Johansson, 2025). Given the group's complex biogeographic history, a similar integrative analysis could be beneficial in Asia, a region that hosts far greater *Parnassius* diversity, with several lineages still unresolved. Applying combined genomic and complementary trait data will be essential to determine whether additional cryptic species occur there and to achieve a consistent, evolutionarily informed taxonomy (Zhao et al., 2022; Lukhtanov et al., 2023; Tian et al., 2023; Condamine, 2018).

.

##############References ordered for summary################

1. Butlin, R. K., Galindo, J., & Grahame, J. W. (2012). Genetics of ecological speciation. *Journal of Evolutionary Biology*, 25(12), 2237–2254.

2. Coyne, J. A., & Orr, H. A. (2004). Speciation. Sunderland, MA: Sinauer Associates.

3. Jiggins, C. D., and J.Mallet. 2000. Bimodal hybrid zones and speciation. Trends Ecol. Evol. 15:250–255.

4. Hewitt, G. (2004). The genetic legacy of the Quaternary ice ages. *Nature*, 405(6789), 907–913.

5. Schmitt, T. (2007). Molecular biogeography of Europe: Pleistocene cycles and postglacial trends. *Frontiers in Zoology*, 4(1), 11.

6. Barton, N., and B. O.Bengtsson. 1986. The barrier to genetic exchange between hybridising populations. Heredity 57:357–376.

7. Barton, N. H. 2020. On the completion of speciation. Philos. Trans. R. Soc. B Biol. Sci. 375:20190530

8. Yukilevich, R. 2012. Asymmetrical patterns of speciation uniquely support reinforcement in Drosophila. Evolution 66:1430–1446

9. Council Directive 92/43/EEC of 21 May 1992 on the conservation of natural habitats and of wild fauna and flora. *OJ L 206, 22.7.1992, pp. 7–50*

10. Gratton, P., Konopiński, M. K., & Sbordoni, V. (2008). Pleistocene evolutionary history of the Clouded Apollo (*Parnassius mnemosyne*): genetic signatures of climate cycles and a 'time-dependent' mitochondrial substitution rate. *Molecular Ecology*, 17(19), 4248–4262.

11. Dincă, V., Montagud, S., Talavera, G., Hernández-Roldán, J., Munguira, M. L., García-Barros, E., Hebert, P. D. N., & Vila, R. (2015). DNA barcode reference library for Iberian butterflies enables a continental-scale preview of potential cryptic diversity. *Scientific Reports*, 5, 12395. https://doi.org/10.1038/srep12395

12. Dincă, V., Dapporto, L., Somervuo, P., Vodă, R., Cuvelier, S., Gascoigne-Pees, M., Huemer, P., Mutanen, M., Hebert, P. D. N., & Vila, R. (2021). High resolution DNA barcode library for European butterflies reveals continental patterns of mitochondrial genetic diversity. *Communications Biology*, 4, 315. https://doi.org/10.1038/s42003-021-01834-7

13. Bolotov, I. N., et al. (2021). *Parnassius nebrodensis*: A threatened but neglected Apollo butterfly species from Southern Europe (Lepidoptera: Papilionidae). *Ecologica Montenegrina*, 40, 140–163.

14. Cotton, A. M., et al. (2021). The correct name for the South Western European species recently separated from *Parnassius mnemosyne* (Linnaeus, 1758) (Lepidoptera: Papilionidae). *Ecologica Montenegrina*, 43, 56–58.

15. Dapporto, L., Menchetti, M., Vodă, R., Corbella, C., Cuvelier, S., Djemadi, I., … Vila, R. (2022). The Atlas of mitochondrial genetic diversity for Western Palearctic butterflies. *Global Ecology and Biogeography*, 31, 2184–2190. https://onlinelibrary.wiley.com/doi/full/10.1111/geb.13579

16.Lukhtanov, Vladimir A., and Evgeny V. Zakharov. "Taxonomic structure and wing pattern evolution in the *Parnassius mnemosyne* species complex (Lepidoptera, Papilionidae)." *Insects* 14.12 (2023): 942.

17. Höglund, J., et al. (2024). A chromosome-level genome assembly and annotation for the clouded apollo butterfly (*Parnassius mnemosyne*): A species of global conservation concern. *Genome Biology and Evolution*, 16(2), evae031.

18. Gratton, P., et al. (2025). Genetic data suggest gene flow within a narrow hybrid zone between two recently separated species in the genus *Parnassius* (Lepidoptera: Papilionidae). *PLoS ONE*, 20(4), e0321742.

19. Nadler, J., Benyamini, D., Bonelli, S., Comay, O., Dapporto, L., Karaçetin, E., Lukhtanov, V., López Munguira, M., Micevski, N., Settele, J., Tzortzakaki, O., Verovnik, R., Warren, M., Wiemers, M.,

20. Cini, Alessandro, et al. "The decline of the charismatic *Parnassius mnemosyne* (L.) (Lepidoptera: Papilionidae) in a Central Italy national park: a call for urgent actions." *Journal of Insect Biodiversity* 16.2 (2020): 47-54.

21.Nadler, J., Benyamini, D., Bonelli, S., Comay, O., Dapporto, L., Karaçetin, E., Lukhtanov, V., López Munguira, M., Micevski, N., Settele, J., Tzortzakaki, O., Verovnik, R., Warren, M., Wiemers, M., Wynhoff, I. & van Swaay, C. 2021. *Parnassius mnemosyne*. *The IUCN Red List of Threatened Species* 2021: e.T174210A122602056. https://dx.doi.org/10.2305/IUCN.UK.2021-1.RLTS.T174210A122602056.en.

Wynhoff, I. & van Swaay, C. 2021. *Parnassius mnemosyne*. The IUCN Red List of Threatened Species 2021:e.T174210A122602056.https://dx.doi.org/10.2305/IUCN.UK.2021-1.RLTS.T174210A122602056.en . Accessed on 18 February 2026.

Araujo, M. B. & M. Luoto. 2007. The importance of biotic interactions for modelling species distributions under climate change. *Global Ecology and Biogeography* 16: 743–753.

Bolotov, Ivan N., Gofarov, Mikhail Yu., Rykov, Alexander M., Frolov, Artyom A., & Kogut, Yaroslava E. (2013). Northern Boundary of the Range of the Clouded Apollo Butterfly *Parnassius mnemosyne* (L.) (Papilionidae): Climate Influence Or Degradation of Larval Host Plants? *Nota Lepidopterologica*, 36, 19–33. https://www.biodiversitylibrary.org/part/147387

Catalan Butterfly Monitoring Scheme (CBMS). Available at: https://www.catalanbms.org/en/especies/pappmn/

Condamine, Fabien L. (2018). Limited by the roof of the world: mountain radiations of Apollo swallowtails controlled by diversity-dependence processes. *Biology Letters* 14(3).

Dapporto, Leonardo, et al. (2024). The genetic legacy of the Quaternary ice ages for West Palearctic butterflies. *Science Advances* 10(38): eadm8596.

Franzén, Markus, and Victor Johansson. (2025). Recent butterfly extinctions in Sweden reveal the inadequacy of site-based protection and the need for landscape-scale management. *Conservation Science and Practice* 7(12): e70188.

Kozak, Krzysztof M., et al. (2015). Multilocus species trees show the recent adaptive radiation of the mimetic *Heliconius* butterflies. *Systematic Biology* 64(3): 505–524.

Lowry, D. B., and B. A. Gould. (2016). Speciation continuum. Elsevier, Amsterdam, The Netherlands.

Mallet, James, et al. (2007). Natural hybridization in heliconiine butterflies: the species boundary as a continuum. *BMC Evolutionary Biology* 7(1): 28.

Marques, Valeria, et al. (2024). The opposed forces of differentiation and admixture across glacial cycles in the butterfly *Aglais urticae*. *Molecular Ecology* 33(7): e17304.

Schmitt, T., Habel, J. C., Zimmermann, M., & Müller, P. (2006). Genetic differentiation of the marbled white butterfly, *Melanargia galathea*, accounts for glacial distribution patterns and postglacial range expansion in southeastern Europe. *Molecular Ecology* 15(7): 1889–1901.

Schmitt, Th., and G. M. Hewitt. (2004). The genetic pattern of population threat and loss: a case study of butterflies. *Molecular Ecology* 13(1): 21–31.

Sean Stankowski, Mark Ravinet. (2021). Defining the speciation continuum. *Evolution* 75(6): 1256–1273. https://doi.org/10.1111/evo.14215

Shaw, K. L., & Mullen, S. P. (2014). Speciation continuum. *Journal of Heredity* 105(S1): 741–742. https://doi.org/10.1093/jhered/esu060

Taberlet, Pierre, et al. (1998). Comparative phylogeography and postglacial colonization routes in Europe. *Molecular Ecology* 7(4): 453–464.

Tian, Xiao, et al. (2023). Amplicon capture phylogenomics provides new insights into the phylogeny and evolution of alpine *Parnassius* butterflies (Lepidoptera: Papilionidae). *Systematic Entomology* 48(4): 571–584.

Westin, Anna, Tommy Lennartsson, and Jan-Olov Bjorklund. (2018). The historical ecology approach in species conservation—Identifying suitable habitat management for the endangered clouded Apollo butterfly (*Parnassius mnemosyne* L.) in Sweden. *AIMS Environmental Science* 5(4).

Zhao, Youjie, et al. (2022). Phylogeny and biogeographic history of *Parnassius* butterflies (Papilionidae: Parnassiinae) reveal their origin and deep diversification in West China. *Insects* 13(5): 406.

Adams, D.C., F. J. Rohlf, and D.E. Slice. 2013. A field comes of age: Geometric morphometrics in the 21st century. Hystrix. 24:7-14.

Adams, D.C., and E. Otarola-Castillo. 2013. geomorph: an R package for the collection and analysis of geometric morphometric shape data. Methods in Ecology and Evolution.4:393-399.

Adams, D.C., and M.L. Collyer. 2024. Extending Phylogenetic Regression Models for Comparing Within-Species Patterns Across the Tree of Life. Methods in Ecology and Evolution. 15:2234-2246.

Baken, E.K., M.L. Collyer, A. Kaliontzopoulou, and D.C. Adams. 2021. geomorph v4.0 and gmShiny: enhanced analytics and a new graphical interface for a comprehensive morphometric experience. Methods in Ecology and Evolution. 12:2355–2363.

Bookstein, F. L. 1991. Morphometric tools for landmark data: geometry and biology. Cambridge Univ. Press, Cambridge.

Collyer, M.L, and D.C. Adams. 2018. RRPP: An R package for fitting linear models to high-dimensional data using residual randomization. Methods in Ecology and Evolution. 9:1772-1779.

Collyer, M.L., and D.C. Adams. 2024. Interrogating Random and Systematic Measurement Error in Morphometric Data. Evolutionary Biology. 51:179-207.

Mitteroecker, P., and K. Schaefer. 2022. Thirty years of geometric morphometrics: Achievements, challenges, and the ongoing quest for biological meaningfulness. American Journal of Biological Anthropology. 178:181-210.

Rohlf, F. J, and D. E. Slice. 1990. Extensions of the Procrustes method for the optimal superimposition of landmarks. Systematic zoology 39:40-59.

2. Methods

2.1 Sampling

P. mnemosyne is a butterfly species with a broad Palearctic distribution, spanning from Kazakhstan in the east to the Pyrenees in the west. Its range extends northward to Russia and southward to Iran, Turkey, the Balkans, and Italy. To capture the genetic diversity across this wide distribution, we studied 66 specimens from key regions, including the Balkans, Italy, Switzerland, Spain, Sweden, Ukraine, and Russia, among others. Of these, 29 specimens originated from west of the contact zone described by Bolotov et al. (2021), representing populations potentially corresponding to *P. turatii,* while the remaining specimens were sampled from east of the contact zone, likely representing *P. mnemosyne* sensu stricto. Additionally, two specimens of *Parnassius ariadne* were used as outgroup taxa. Butterfly bodies were stored in 99% ethanol at −20°C, and wings were kept separately as vouchers. While more specimens were initially used, some were excluded due to insufficient sequencing coverage in later steps.

2.2 ddRADseq library preparation

To obtain genome-wide representation, we applied a double-digest restriction-associated DNA (ddRAD) sequencing protocol. Genomic DNA (gDNA) was extracted from half of the thorax using the DNeasy Blood & Tissue Kit (Qiagen), and its quantity was assessed with the PicoGreen kit (Molecular Probes). Whole-genome amplification was performed using the REPLI-g Mini Kit (Qiagen) to enhance gDNA yield, followed by a second quantification with the PicoGreen kit. Each sample was digested using a combination of restriction enzymes: 500 ng of DNA was treated with 1 µL PstI, 2 µL MseI, and 5 µL of CutSmart Buffer (New England Biolabs), with water added to reach a final volume of 50 µL. Digestion was conducted at 37°C for 2 hours, after which samples were frozen to deactivate the enzymes. DNA purification was carried out using AMPure XP magnetic beads (Agencourt) on a Biomek automated liquid handler (Beckman Coulter), with a final elution volume of 40 µL. DNA concentrations were reassessed with PicoGreen, and these values were used for sample pooling. Adapter ligation was performed to enable individual sample identification. Each reaction included 5 µL T4 DNA Ligase Buffer (New England Biolabs), 1 µL T4 DNA Ligase (New England Biolabs), 0.6 µL rATP (Promega), 5 µL P1 adapter (50 nM), 5 µL P2 adapter (50 nM), and 2.4 µL water. The P1 adapter contained 45 unique Illumina primer sequences, 5 bp barcodes, and a TGCA overhang complementary to the PstI sticky end. The P2 adapter included Illumina primer sequences with AT overhangs to match the MseI cut site and incorporated a 'divergent-Y' structure to prevent amplification of fragments flanked by MseI cut sites. The ligation reaction was incubated at 22°C for 1 hour, followed by enzyme deactivation at 65°C for 20 minutes. For library preparation, 200 ng of each sample was pooled into three groups, each with a final volume of approximately 450 µL. The pooled samples underwent purification with AMPure XP magnetic beads, followed by size selection at 300 bp using the BluePippin system (Sage Science). Subsequently, PCR amplification was conducted using primers RAD1.F (5′ -AATGATACGGCGACCACCGAGATCTACACTCTTTCCCTACACGACG-3′) and RAD2.R (5′-CAAGCAGAAGACGGCATACGAGATCGTGATGTGACTGGAGTTCAGACGTGTGC -3′). The reaction mixture (60 µL total volume) consisted of 9 µL water, 30 µL Phusion High-Fidelity PCR Master Mix (Finnzymes), 3 µL of each primer (10 mM), and 15 µL DNA.

The PCR conditions included an initial denaturation at 98°C for 30 seconds, followed by 16 cycles of denaturation at 98°C for 10 seconds, annealing at 60°C for 30 seconds, and extension at 72°C for 40 seconds, with a final extension at 72°C for 5 minutes. The amplified products were purified using AMPure XP magnetic beads, and DNA concentrations were re-evaluated with PicoGreen. Final size distribution and concentration of the pooled libraries were assessed using a Bioanalyzer (Agilent Technologies). Equimolar amounts of the libraries were pooled and sequenced on an Illumina HiSeq 2500 PE 100 platform at the FIMM Technology Center (Helsinki, Finland). The resulting demultiplexed FASTQ data were deposited in the NCBI Sequence Read Archive (SRA) under accession numbers SRR24894924-SRR24895002, associated with BioProject PRJNA980705.

2.3 Data processing

To process the sequencing data, we employed IPYRAD v0.7.23 (Eaton & Overcast, 2020) for initial filtering, SNP detection, and alignment. The genome of *P. mnemosyne* (*Parnassius_mnemosyne*_n_2023_11; GCA_963668995.1) was used as a reference, obtained from the ERGA project (Höglund et al., 2024). Key parameters were customized to suit the study's requirements: the assembly mode was configured to "reference-based," the data type was set to "pairddrad," and the restriction enzyme overhangs were specified as TGCAG and TAA. Additional adjustments included setting a minimum read length of 70 base pairs after trimming, requiring loci to be present in at least four samples, and limiting both the number of SNPs and indels per locus to 20 and 8, respectively. The resulting dataset consisted of 91,036 loci spanning a total of 19,837,673 base pairs, which included 1,514,746 high-quality SNPs.

2.4 Population genetic structure and phylogenetic inference

We assessed population genetic structure using Principal Component Analysis (PCA) and Bayesian clustering. The PCA was performed after filtering the dataset to exclude samples of *P. ariadne*. Additional filtering steps were conducted with VCFtools v0.1.17 (Danecek et al., 2011), where we removed indels, excluded SNPs with more than 50% missing data, and retained variants with a minimum allele frequency of 0.008. To focus on unlinked SNPs, we applied variant pruning using PLINK v1.90b6.24 (Chang et al., 2015), with parameters set to a window size of 50 SNPs, a step size of 10 SNPs, and an r^2 threshold of 0.1. These steps yielded a final dataset of 15,041 SNPs. PCA computation was performed in PLINK v1.07 (Purcell et al., 2007) and visualized in R (R Core Team, 2021) using the tidyverse package (Wickham et al., 2019).

For Bayesian clustering, we analyzed genetic structure with STRUCTURE v2.3.4 (Pritchard et al., 2000). We tested values of K ranging from 1 to 6, using a burn-in of 75,000 iterations followed by 200,000 Markov Chain Monte Carlo (MCMC) replicates. Each K was run ten times, and the outputs were averaged using CLUMPAK v1.1 (Kopelman et al., 2015). The optimal K was determined with the Evanno method in STRUCTURE HARVESTER v0.6.94 (Earl & vonHoldt, 2012).

To infer phylogenetic relationships among the 63 individuals in the dataset, we constructed a maximum likelihood phylogeny using IQTREE v2.1.2 (Nguyen et al., 2015). The analysis employed the TVM+F+R2 substitution model, which was selected automatically by ModelFinder (Kalyaanamoorthy et al., 2017), and included 1,000 bootstrap replicates. The resulting phylogeny was visualized, and bootstrap support was assessed with FIGTREE v1.4.2 (Rambaut & Drummond, 2012).

2.5 Gene flow analysis

To investigate patterns of differential introgression between the populations belonging to taxa *mnemosyne* and *turatii*, we conducted an ABBA-BABA analysis (also referred to as D-statistics; Durand et al., 2011). The analysis was performed using a variant calling file containing 384,718 SNPs from a dataset that had been filtered to exclude contaminants. Calculations were carried out using the DTRIOS module within the DSUITE software package (Malinsky, 2019). DTRIOS employs a standard block-jackknife procedure to evaluate whether the D-statistic deviates significantly from zero, which represents the null hypothesis of no introgression. The ordering of P1 and P2 ensures that nABBA ≥ nBABA, meaning that a significant result would identify the species assigned as P2 as the one potentially introgressed.

We analyzed a dataset of 384,718 variants using Dsuite Dtrios. The analysis included three sets (excluding the outgroup), and D and $f_4$$f_4$-ratio statistics were calculated for four trio combinations. Two of these trios focused on populations in the contact zone, while the other two targeted potential introgression events suggested by the structure analysis and PCA.

2.6 Ecological Niche Modeling

We compiled occurrence data for *P. mnemosyne* sensu lato from the Global Biodiversity Information Facility (GBIF) covering the years 1979 to 2013. The dataset contained 6,758 records, of which 3,218 were assigned to the taxon *mnemosyne* and 3,540 to the taxon *turatii* based on the lineage distributions described by Bolotov et al. (2021) and analysed separately. Data were downloaded using the occ_download function from the rgbif R package (v3.7.2; Chamberlain & Boettiger, 2017), specifying a geographic region bounded by longitudes −11.64551° to 48.20801° and latitudes 29.26758° to 72.1582°. We excluded records with geospatial issues and restricted thbueno e query to this time frame. To reduce spatial sampling bias, we applied a thinning procedure using the spThin R package (v0.2.0; Aiello-Lammens et al., 2015), maintaining a minimum distance of 10 km between occurrence points.

Environmental predictor variables were selected to capture key climatic factors shaping species distributions. We used 19 bioclimatic variables at ~10 km resolution (5 arc-minutes) from the Paleoclim database (Brown et al., 2018) for the present (1979–2013), as well as paleoclimatic data from the Last Glacial Maximum (~21,000 years ago; Karger et al., 2021). To address collinearity, we calculated Pearson correlation coefficients and retained only variables with correlations below |0.7|. The final predictor set included mean diurnal range (bio2), minimum temperature of the coldest month (bio6), mean temperature of the wettest quarter (bio8), precipitation of the coldest quarter (bio19), and precipitation of the warmest quarter (bio18), prepared as raster layers for modeling.

Species distribution modeling was performed using the biomod2 R package (v3.5.1; Thuiller et al., 2023) to estimate habitat suitability under present and historical climates. We complemented presence data with pseudo-absence points by randomly selecting five independent sets of 1,000 points across the study area to reflect the environmental background. Six modeling algorithms were used: Generalized Linear Models (GLM), Generalized Additive Models (GAM), Multiple Adaptive Regression Splines (MARS), Classification Tree Analysis (CTA), Flexible Discriminant Analysis (FDA), and Random Forests (RF). We trained models on 80% of the occurrence data and assessed performance using the True Skill Statistic (TSS), with ten cross-validation replicates to ensure robust predictions.

For each time period, final habitat suitability maps were generated by averaging models with TSS > 0.7 to produce consensus projections. Importantly, all analyses were conducted

separately for *P. mnemosyne* and *P. turatii* to explicitly compare their ecological niches and potential range differences.

2.7 Demographic Modeling Inference

We used the dadi software (Gutenkunst et al., 2009) and dadi_pipeline v3.1.5 (Portik et al., 2017) to reconstruct demographic history and gene flow patterns among *Parnassius* populations based on the joint site frequency spectra (JSFS). The JSFS was built using the easySFS tool from a filtered ddRAD-seq. To ensure data quality, we retained only unlinked SNPs and excluded loci with over 50% missing data, minimizing biases from linkage disequilibrium and low-quality genotypes.

We tested four demographic models: (1) split_uni_mig_adjacent_var2 (split with unidirectional migration between adjacent populations), (2) split_sym_mig_adjacent_var2 (split with symmetric migration), (3) admix_origin_no_mig (admixture origin without ongoing migration), and (4) split_nomig (pure isolation with no migration). Each model was evaluated twice, switching the population ordering in the input to test whether the Pyrenean population is more closely related to *P. turatii* or *P. mnemosyne*, directly addressing uncertainties in its phylogenetic placement. Model implementation and optimization were carried out using dadi_pipeline v3.1.5 (Portik et al., 2017), with four iterative rounds of parameter fitting. Replicates achieving the highest log-likelihoods were used to initialize subsequent rounds. Optimization relied on the Nelder–Mead algorithm (optimize_log_fmin), following dadi_pipeline's defaults: 10, 20, 30, or 40 replicates per round, with up to 3, 5, 10, or 15 iterations per replicate. Model selection was based on the Akaike Information Criterion (AIC), selecting the model with the lowest AIC as the best fit.

To convert estimated parameters—ν (relative population size), m (migration rate), and t (divergence time)—into biological units, we used the θ (theta) estimate from dadi. The ancestral effective population size (Nref) was calculated as $N_{ref} = \theta / (4L\mu)$, where L is the number of analyzed sites, determined as the proportion of retained SNPs (31,255) relative to the total called SNPs (1,514,746 across ~19,837,673 base pairs), and μ is the per-site per-generation mutation rate. We used a mutation rate of 2.9×10^{-9} per base pair per generation, based on *Heliconius melpomene* (Keightley et al., 2015), widely used in Lepidoptera. We assumed a generation time of 1 year (one generation per year). Final estimates included $N = \nu \times N_{ref}$, migration rates per generation as $M = m / (2N_{ref})$, and divergence times in years as $T = 2t \times N_{ref} \times g$, where g is generation time. These conversions provided biologically meaningful estimates of population sizes, migration rates, and divergence times, offering detailed insight into the evolutionary and demographic processes shaping the *P. mnemosyne* complex.

2.8 Geometric morphometrics

To characterize the shape of wing scales we used geometric morphometrics (Adams et al. 2013; Mitteroecker and Schaefer 2022). First, we selected five scales from the wings of each of 42 individuals, and digitized the locations of four landmarks demarcating the corners of each scale to represent its shape (Fig 4B). We then performed a Generalized Procrustes Analysis (Rohlf and Slice 1990) to eliminate nonshape variation and align the 210 scales to a common coordinate system. The aligned Procrustes coordinates were then used in all statistical analyses. Specifically, we performed a principal components analysis (PCA) to visualize overall patterns of scale shape variation. Thin-plate spline deformation grids (Bookstein 1991) were then used to generate graphical representations of scale shapes for the means of each group. We then compared scale shapes across groups, using a permutation-based hierarchical multivariate analysis of variance. Residual randomization permutation procedures (RRPP, sensu Collyer and Adams 2018) were performed within

individuals to account for the nonindependence among scales obtained from the same individual (for related procedures see Adams and Collyer 2024; Collyer and Adams 2024). Pairwise comparisons among groups were also conducted using the same permutation schedule (Collyer and Adams 2018). Additional analyses comparing species distinctness based on scale shape are found in the Supplementary. All analyses were conducted in R, using the geomorph (Adams and Otarola Castillo 2013; Baken et al. 2021) and RRPP (Collyer and Adams 2018) packages.

2.9 **Cuticular Hydrocarbon Extraction and GC-MS Analysis**

Cuticular hydrocarbons (CHCs) were extracted from the same individuals used for morphometric and genetic analyses. For each specimen, the portion of the hindwing near the androconium was excised using clean scissors and immersed in 200 µL of pentane for 10 min at room temperature. The solvent was then evaporated to dryness under a gentle stream of nitrogen. The extract was resuspended in pentane, and 2 µL of this solution was injected into the Gas Chromatography-Mass Spectrometry (GC-MS).

Chemical analyses were performed using an Agilent 7820A gas chromatograph coupled to an HP 5977B mass selective detector (Agilent Technologies, Palo Alto, CA, USA). The GC was equipped with a non-polar capillary column (J&W DB-5ms fused silica, 30 m × 0.25 mm x 0.10 µm, Agilent Technologies). Injections were performed in splitless mode (1 min purge valve off). The injector port was set at 280°C, and the carrier gas was helium (at 15 psi head pressure). The oven temperature program was as follows: 70°C held for 3 min, increased by 15°C/min to 150°C (held for 3 min), and then increased by 5°C/min to a final temperature of 310°C (held for 4.667 min). The mass spectrometer was operated in electron impact (EI) ionization mode at 70 eV. The transfer line, ion source, and quadrupole temperatures were set at 300°C, 230°C, and 150°C, respectively. Mass spectra were acquired in full scan mode in the range of 50–550 m/z. Data acquisition and analysis were performed using the Agilent Masshunter Workstation software (version B.07.00).

Compound identification was achieved by comparing the mass spectra of the eluted peaks with those present in the NIST library and by analyzing their fragmentation patterns. To confirm the identity of linear alkanes and calculate retention indices, a standard mixture of linear alkanes was injected under the same analytical conditions. We focused our analysis specifically on cuticular hydrocarbons; therefore, non-CHC compounds and contaminants were excluded from the dataset. Peak areas were integrated to estimate relative compound abundance. To ensure dataset consistency, peaks that co-eluted in some samples but appeared separated in others were summed and treated as a single variable.

An initial set of 43 CHCs was identified (Table XX). Since the integration parameters were set to exclude negligible signals (implicitly filtering out peaks with <1% relative abundance), no further post-hoc abundance filter was applied. However, to ensure robustness, only compounds found in at least 25% of the samples were retained. This final filtering step resulted in a dataset of 30 CHCs used for subsequent statistical analyses.

Chemical discrimination and chemical data preprocessing

Cuticular hydrocarbon (CHC) peak areas were used as compositional chemical profiles. To account for the compositional nature of the data, zero values were replaced using a count zero multiplicative (CZM) approach implemented in the cmultRepl function of the zCompositions package, and data were subsequently transformed into Aitchison geometry using the centred log-ratio (CLR) transformation (using the clr function of the compositions R package). Analyses were restricted to male specimens to avoid sex-related chemical variation.

For descriptive and exploratory purposes, specimens were assigned to a combination of species and geographic regions. In particular, we identified two contact populations—*P.*

turatii from the Alps and *P. mnemosyne* from the same area—, defined as the populations within 100km from the known contact point (46.0 lat; 12.0 long). Non-contact populations for each species were the Pyrenees and Western Alps–Italian Peninsula-Sicily populations for *P. turatii*; and North-Eastern Europe populations for *P. mnemosyne*.
To assess whether a combination of chemical compounds could discriminate between *P. mnemosyne* and *P. turatii*, we performed sparse Partial Least Squares Discriminant Analysis (sPLS-DA) using the splsda function of the mixOmics R package. Unlike unsupervised ordinations, sPLS-DA explicitly maximizes covariance between chemical profiles (X) and species identity (Y), and is therefore appropriate to test the a priori discriminability of species based on CHC composition. We fitted a two-component sPLS-DA model, retaining a maximum of ten compounds per component which assured to avoid overfitting since more than 10 specimens per variable in each component were included. SPLSDA allowed both dimensionality reduction and variable selection. Model performance on specimens from different species and regions was evaluated using leave-one-out cross-validation (LOO), implemented via the perf() function in mixOmics with centroid-based distances. For each specimen, posterior class membership probabilities were extracted and the predicted class was assigned as the class with the highest probability. Classification accuracy was calculated as the percentage of correctly classified specimens, both overall and separately for each geographic group. This allowed us to assess whether classification performance differed between contact and non-contact populations.

To obtain an unsupervised low-dimensional representation of chemical variation, we performed a principal component analysis (PCA) on the CLR-transformed data (prcomp, centred but not scaled). PCA was used to obtain an orthogonal representation of chemical variation, thereby reducing redundancy among correlated compounds before calculating interspecific distances. Scores on the first two principal components (PC1–PC2; or the set of PCs specified a priori) were used as an Euclidean embedding of chemical profiles. Pairwise chemical distances were calculated as Euclidean distances between individuals in this PCA space.

For each individual, geographic distance to the contact point (46.0 lat; 12.0 long) was computed using great-circle distances (earth.dist from the fossil package). This yielded an individual-level predictor variable (dist_contact, in km).

To quantify interspecific chemical divergence while focusing on comparisons between species, we extracted the rectangular block of the pairwise distance matrix corresponding to distances between P. mnemosyne and P. turatii individuals (mnemosyne × turatii). We then obtained, for each interspecific pairwise comparison, the chemical distance in PCA space (chemDist) and the focal individual's distance to the contact point (contactDist).

Because each individual contributes to multiple pairwise comparisons, we represented the data in two complementary sets: mnemosyne-as-focal: each mnemosyne individual paired with all turatii individuals, with contactDist defined as that mnemosyne individual's distance to the contact zone; and turatii-as-focal: each turatii individual paired with all mnemosyne individuals, with contactDist defined as that turatii individual's distance to the contact zone. These two sets were combined into a single dataset with four key variables: interspecific chemical distance (chemDist), distance from the contact zone (contactDist), focal species: mnemosyne vs turatii (Species) and ID of the focal specimen (id_focal). As each observation corresponds to a chemical distance between P. mnemosyne and P. turatii, species identity does

not represent an independent grouping factor but only specifies which individual provides the distance to the contact zone; accordingly, models focused on distance effects rather than species main effect.

Pairwise distances are not independent because each focal individual appears repeatedly across multiple pairwise comparisons. To account for this non-independence, we fitted a Gaussian mixed model using the gam function of the mgcv R package with a random intercept for the focal individual:
chemDistcontactDist+contactDist:Species+(1 | id_focal)

Models were fitted using REML. The main effect of contactDist tests whether interspecific chemical divergence changes with distance from the contact zone, the main effect of Species tests for overall differences between focal-species views, and the interaction tests whether the distance–divergence relationship differs between the two focal species.

To visualise fitted trends, we generated marginal predictions of ChemDist along the observed range of contactDist, separately for each focal species. Predicted values and 95% confidence intervals were plotted in a mirrored layout: the *P. turatii* trend was displayed on the negative x-axis (left), and the *P. mnemosyne* trend on the positive x-axis (right), with the contact zone centred at x = 0. This representation allows direct visual comparison of distance-dependent trends between species while keeping the contact point as a common reference.

2.10 *Wolbachia* infection

To assess the potential influence of *Wolbachia* on genetic differentiation, we screened for this endosymbiotic bacterium, which is known to cause reproductive alterations such as male-killing and cytoplasmic incompatibility (Jiggins, 2003; Werren et al., 2008). Sequence data were analyzed using CENTRIFUGE v1.0.4 (Kim et al., 2016), a rapid and sensitive tool for bacterial sequence detection (Hinojosa, Koubínová et al., 2019; Hinojosa, Monasterio et al., 2019). Because some reads did not align to the *P. mnemosyne* reference genome, we performed a de novo assembly using IPYRAD v0.7.23 (Eaton & Overcast, 2020) specifically to retain potential symbiont sequences that would otherwise be discarded. The assembled loci were then analyzed in CENTRIFUGE using the complete bacterial and viral genome index from the NCBI BLAST nucleotide database, enabling the identification and classification of *Wolbachia* sequences.